

Mechanical limits of viral capsids

Mathias Buenemann^{*}, Peter Lenz^{* †}

^{*}Fachbereich Physik, Philipps-Universität Marburg, D-35032 Marburg, and [†]Center for Theoretical Biological Physics, University of California at San Diego, La Jolla, California 92093-0374, USA

Submitted to Proceedings of the National Academy of Sciences of the United States of America

We study the elastic properties and mechanical stability of viral capsids under external force-loading with computer simulations. Our approach allows the implementation of specific geometries corresponding to specific phages such as $\phi 29$ and CCMV. We demonstrate how in a combined numerical and experimental approach the elastic parameters can be determined with high precision. The experimentally observed bimodality of elastic spring constants is shown to be of geometrical origin, namely the presence of pentavalent units in the viral shell. A criterion for capsid breakage is defined, which explains well the experimentally observed rupture. From our numerics we find for the dependence of the rupture force on the Föppl-von Kármán (FvK) number γ a crossover from $\gamma^{2/3}$ to $\gamma^{1/2}$. For filled capsids high internal pressures lead to a stronger destabilization of viruses with a buckled ground state than unbuckled ones. Finally, we show how our numerically calculated energy maps can be used to extract information about the strength of protein-protein interactions from rupture experiments.

thin shells | membranes | biomaterials

Bacteriophage capsids have astonishing elastic properties. They withstand extreme internal pressures exerted by their densely packed DNA. DNA packaging experiments on phage $\phi 29$ [1] and theoretical arguments [2, 3, 4, 5, 6] imply that phage capsids store their DNA under ~ 50 atm. This pressure is necessary to inject the DNA into the prokaryotic host cell [7]. It has been shown experimentally that the ejection pressure from λ -phages is ~ 20 atm [8]. The remarkable robustness under high pressures motivated recent nanoindentation studies [9], which showed that capsids also resist external point forces up to ~ 1 nN.

In contrast, viruses that infect eukaryotic cells, e.g. CCMV and polyoma, penetrate their host cell. Their DNA is released by subsequent disassembly of the shell. Correspondingly, these viruses do not store their DNA under high pressure. Nevertheless, their resistance to external forces is remarkably strong [10].

Viral capsids are composed of a small number of different proteins, which cluster to morphological units (“capsomers”). These units are put together in a highly regular fashion described by the “quasi-equivalence” principle by Caspar and Klug [11]. Due to the presence of capsomers the surface of capsids has a discrete structure. Mathematically, these capsomers correspond to the vertices of a regular triangulation of a sphere. For such a triangulation the number of vertices V , connecting edges E , and associated faces F have to fulfill Euler’s theorem $F - E + V = 2$. This theorem implies that capsids of icosahedral symmetry have 12 pentavalent morphological units (“pentamers”) embedded in an environment of hexavalent units (“hexamers”).

Viral capsids can undergo elastic and bending deformations. Generally, the elastic properties of such thin shells (of typical length scale R) depend only on a single dimensionless parameter, the FvK number $\gamma \equiv R^2 \kappa_e / \kappa_b$ set by the ratio between elastic modulus κ_e and bending rigidity κ_b . It has been shown in Ref. [12], that at a critical $\gamma_b = 154$ spherical shells undergo a buckling transition, in which the shell acquires a more faceted shape. This transition is caused by large strains associated with the pentamers which are reduced upon

buckling into a conical shape.

Typical γ values of viral shells lie in the range from below the buckling threshold (e.g. alfalfa mosaic virus with $\gamma \simeq 60$ [13]) up to several thousand (e.g. phage $T4$ with $\gamma \simeq 3300$ [14]). An extreme example is the giant mimivirus (diameter of $\simeq 600$ nm) with a FvK number $\gamma \simeq 20000$ [15]. Even higher γ -values are possible for artificial capsules such as vesicles with crystallized lipid membrane [16] ($\gamma \sim 10^5$) or polyelectrolyte capsules [17] ($\gamma \sim 10^6$).

The elastic properties of capsids can be probed in scanning-force microscopy (SFM) experiments [9, 10]. Depending on the strength of loading two regimes are explored. Small forces lead to a completely reversible deformation of capsids. Here, the linear and nonlinear regime of thin spherical shell elasticity can be studied. In this regime the deformations explore the *global* elastic properties. Larger forces (> 1 nN) cause irreversible changes in the shell structure commonly attributed to bond rupture. Rupturing studies therefore give information about the molecular interactions between capsomers thus elucidating *local* features of shell mechanics.

Viral shells have also been the subject of numerical investigations. The dependence of virus shape on the FvK number was analyzed in Ref. [12]. Only recently, the elasticity of capsids has come into the focus of numerical studies [18] which are based on a discretization scheme introduced for crystalline membranes in Ref. [19]. In other approaches, the shells are directly built up of proteins [20] or capsomers [21] with specified (spatially varying) interactions. On this basis the stability of capsids against internal pressure has been studied [22].

Here, we generalize a numerical approach developed for the investigation of vesicles [23] to viral capsids. The big advantage of our method is its applicability to arbitrary geometries. In particular, our discretization of the bending energy does not depend on the underlying triangulation of the viral surface. Therefore, our method produces highly stable and reliable results even under high local strain which allows us to investigate the rupture of mechanical shells. In our simulations, we can systematically vary the elastic moduli and geometry of the capsids and probe their mechanical response to external disturbances. We can even implement specific geometries, corresponding to specific phages and viruses, and determine (by a direct comparison with experimental indentation experiments) with high precision their elastic parameters, such as linear and nonlinear spring constants, and the FvK number. In our simulations, we are also able to access features which are not observable in experiments. For example, by measuring the local strain we are able to determine numerically the spatial distribution of rupture probabilities across the capsid surface. We will show that experimental deviations from this distribution may be used to draw conclusions about the spatial variation of protein binding strength.

Conflict of interest footnote placeholder

This paper was submitted directly to the PNAS office.

Abbreviations: FvK, Föppl-von Kármán number

©2006 by The National Academy of Sciences of the USA

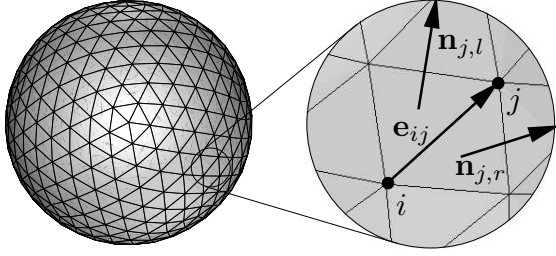


Fig. 1. The viral structure is represented by a triangulated sphere. The pentavalent vertices represent the centers of the pentameric units. Vertices are connected by elastic bonds with spring constant $\tilde{\kappa}_e$. The local mean curvature is calculated from the normals of neighboring facets and their shared edge.

This paper is organized as follows: after a short summary of the numerical methods, we first study the global response of capsids to externally applied point forces. The numerical results for (empty) $\phi 29$ and CCMV are compared with experimental data. Next, we analyze the local, irreversible response to indentation forces and we discuss the dependence of local rupture-probability on the geometry of the capsid. Finally, our analysis is extended to filled capsids whose elastic parameters and mechanical stability is studied in the last 2 sections.

Methods

We have performed numerical minimization simulations of triangulated surfaces representing the surface of capsids with elastic (stretching) and bending energy. In our (small mesh-size) triangulation every capsomer is represented by several vertices. Therefore, these units also have some flexibility and elasticity. Such a discretization is suitable to determine the shape of viral shells [12] and yields results which do not depend on the number of vertices (in contrast to coarse triangulations in which each capsomer is represented by a single vertex [18]). The triangulation represents the underlying icosahedral (quasi-)symmetry of the capsid. In particular, the pentavalent vertices correspond to the centers of the pentamers.

In our model, the vertices are connected by harmonic springs. Any deviation from the preferred inter-vertex distance l gives rise to an elastic energy [19],

$$E_e = \frac{\tilde{\kappa}_e}{2} \sum_{\langle i,j \rangle} (l - |\mathbf{r}_i - \mathbf{r}_j|)^2, \quad [1]$$

where vertex i is at position \mathbf{r}_i and the sum extends over nearest neighbor pairs only. $\tilde{\kappa}_e$ is related to the 2D Young modulus κ_e via $\tilde{\kappa}_e = \sqrt{3}\kappa_e/2$.

The bending energy is given by

$$E_b = \kappa_b \sum_i \frac{H_i^2}{A_i}, \quad [2]$$

where the sum extends over all vertices i . Here, A_i is the area assigned to the i -th vertex given by 1/3 of the area of all adjacent triangles. H_i is the mean curvature of vertex i (with coordination number z_i) given by [23]

$$H_i = \frac{1}{2} \sum_{j=1}^{z_i} \frac{\mathbf{e}_{ij} \cdot (\mathbf{n}_{j,l} \times \mathbf{n}_{j,r})}{|\mathbf{n}_{j,r}| |\mathbf{n}_{j,l}| + \mathbf{n}_{j,r} \cdot \mathbf{n}_{j,l}}, \quad [3]$$

with $\mathbf{e}_{ij} \equiv \mathbf{r}_i - \mathbf{r}_j$, and $\mathbf{n}_{j,l}$ and $\mathbf{n}_{j,r}$ are the non-normalized surface vectors of the facets left and right of the edge connecting vertex i and j , see Fig. 1.

Starting from a triangulated sphere the shape of minimal energy is found by minimizing the total energy $E = E_e + E_b$ using a conjugate gradient algorithm [24]. In order to simulate the SFM-experiments mentioned in the introduction vertices i at the point of loading were moved away from their equilibrium position \mathbf{r}_i . We thus work in an ensemble of prescribed indentation \mathbf{X} rather than in an ensemble of applied force. All vertices are constrained to lie above a (virtual) plane at $z = 0$. The shape of the triangulated surface under these constraints is again found by minimizing the total energy.

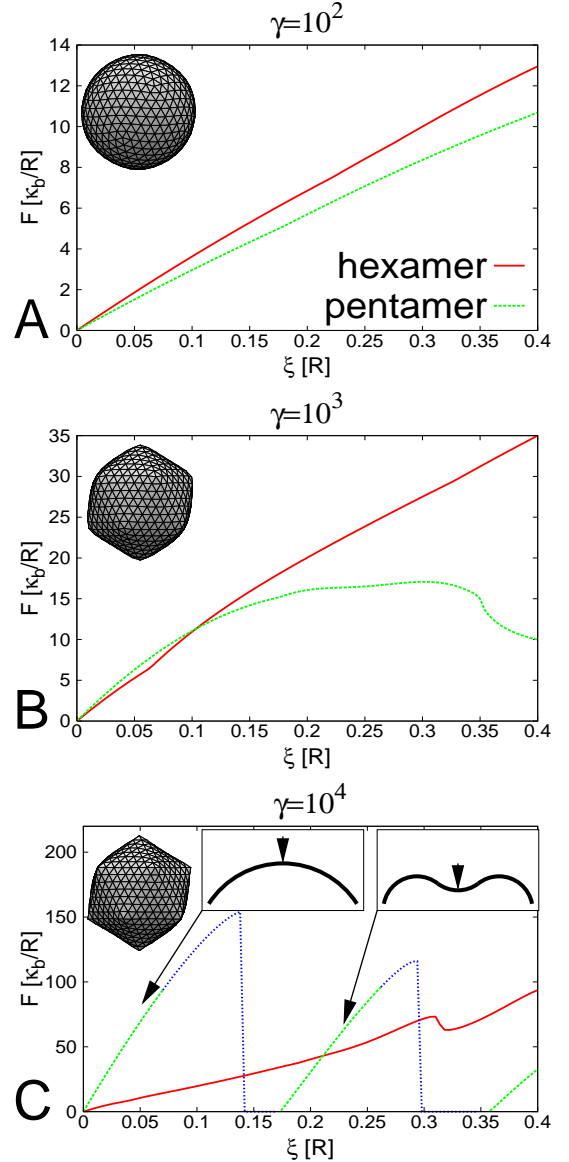


Fig. 2. Force-distance relations of locally deformed viral shells. For small γ the force-distance relation is linear $F \sim \xi$ for the full range of applied forces (A). Above the buckling threshold the structural inhomogeneity of the capsid material is reflected by the increasing differences in the elastic response of pentamers and hexamers (B) and (C). Above $\gamma \approx 1000$ the inversion transition of pentamers (see Fig. 4B) causes softening, which leads to a decrease in $F(\xi)$. The influence on hexamers is much weaker. At higher γ pentamers may even snap into a new stable inverted configuration, which leads to discontinuities of $F(\xi)$. The dotted blue line in (C) represents metastable conformations which have a higher energy than stronger deformed ones. Hexamers do not show a discontinuous inversion transition.

The shapes of bacteriophage $\phi 29$ and the CCMV plant virus have been quantitatively characterized by Cryo-EM and X-ray studies [25, 26]. Phage $\phi 29$ has an average equatorial radius $R \simeq 21\text{nm}$ and a shell thickness of $h \simeq 1.6\text{nm}$. Its FvK number is $\gamma \approx 11(R/h)^2 \simeq 2000$ implying that the shape of $\phi 29$ is noticeably buckled. For CCMV the corresponding values are $R \simeq 12\text{nm}$ and $h \simeq 2.5\text{nm}$. Thus, $\gamma \simeq 300$ and CCMV is slightly buckled.

Results and Discussion

Spring Constants. As mentioned in the introduction loading with small forces probes the global elastic behavior of viral shells. Here, we analyze the influence of internal structure on the elastic response of capsids by comparing the numerical simulations with analytical results for small deformations. Furthermore, we extract the values of the elastic moduli of $\phi 29$ and CCMV by a direct comparison of numerical and experimental force-distance relations.

In a first step we have numerically calculated force-distance curves for viruses indented by a distance $X \equiv \xi R$ for $0 \leq \xi \leq 0.4$ (varying with step-size $\Delta\xi = 1/250$). By minimizing the total energy the (dimensionless) force F is obtained by $F = -\Delta E/(\kappa_b \Delta\xi)$,

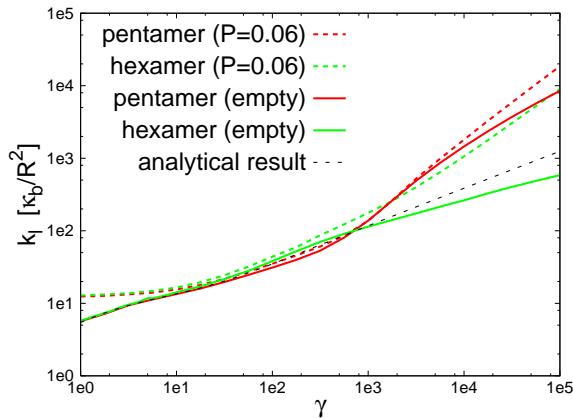


Fig. 3. Linear spring constants as a function of γ for empty (solid lines) and filled (dashed lines) icosahedral capsids. The black dashed line represents the analytical solution (see suppl. mater.). For $\gamma < \gamma_b$ the spring constants of the empty capsid follow closely the theoretical prediction. Above γ_b , the spring constant of hexamers $\sim \gamma^{1/3}$. Pentamers become stiffer and (roughly) $\sim \gamma^1$. Generally, filled capsids have higher spring constants. Data for the filled capsids is for $p = 0.06\kappa_e/R$ (internal pressure of phage $\phi 29$).

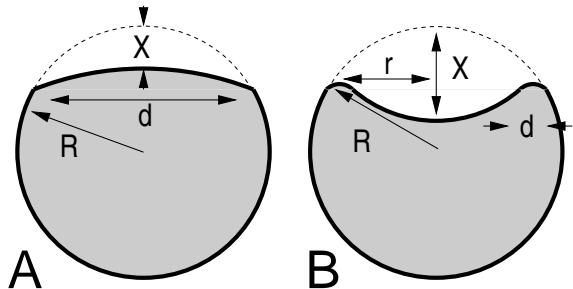


Fig. 4. Global response of elastic spherical capsids to local deformations. (A) For small indentations only the top of the shell is flattened giving rise to a linear force-distance relation. (B) At a critical indentation $\xi_c \sim h/R$ the capsid partially inverts its shape.

where ΔE is the change in total energy caused by the increase $\Delta\xi$ in X . Both hexamers and pentamers were displaced. The indented hexamers discussed here all lie in the center of the facet spanned by their three neighboring pentamers.

As can be seen from Fig. 2 the elastic response of the capsid to the deformation strongly depends on the ratio of bending and elastic energy characterized by the FvK number γ . For small γ capsids have a nearly spherical shape [12] and behave like homogeneous continuous shells. For $10 < \gamma < 500$ the (dimensionless) linear spring constants K_l of both hexameric and pentameric regions follow a square root law for sufficiently small $\xi < \xi_c(\gamma)$

$$F = K_l \xi \equiv 4\sqrt{\gamma} \xi, \quad [4]$$

see Fig. 3. The transition to the nonlinear regime (at $\xi = \xi_c$) takes place at smaller ξ_c the larger γ , see Fig. 2A and B. For small FvK number $\gamma \sim (R/h)^2$ corrections to thin shell theory of order h/R become relevant.

For $\gamma > 500$ the capsid has a strongly faceted shape since the 12 disclinations buckle. Due to this structural inhomogeneity the elastic response of pentamers and hexamers is different, i.e. pentamers generally become stiffer than hexamers with increasing γ . Furthermore, the abrupt shape transformation shown in Fig. 2C only occurs for loading on pentamers.

As Fig. 3 shows, the difference between the spring constants for pentamers and hexamers increases with increasing γ . At $\gamma \approx 2000$ the spring constants are already well separated explaining the experimentally measured bimodality of spring constants of $\phi 29$ [9]. From our numerical data we find $K_l \sim \gamma^{1/3}$ for hexamers and $K_l \sim \gamma^1$ for pentamers. When loading on pentamers is parallel to ridges then $K_l \sim \gamma^{5/6}$ in agreement with the findings of Refs. [27, 28].

The elastic behavior of spherical capsids under axial point force can be understood by simple scaling arguments [29] of an elastic sphere with energy $E = E_e + E_b$. For small indentations X the top of the sphere is flattened in a circular region of diameter d , see Fig. 4A. In the flattened region the radius of curvature $\sim d^2/X$ and meridians are compressed by an amount $\sim \xi$. In equilibrium one then finds $d \sim R/\gamma^{1/4}$ yielding a total energy $E/\kappa_b \sim \gamma^{1/2}\xi^2$ of the deformed sphere. Thus, the force-distance relation is linear with $K_l \sim \gamma^{1/2}$.

In fact, a more rigorous analysis of the linear regime yields [30]

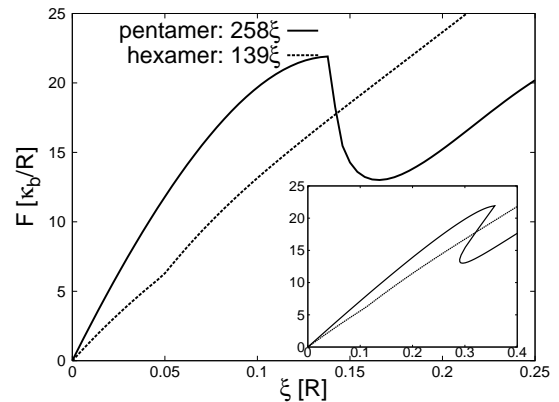


Fig. 5. Numerical indentation experiment on $\phi 29$ (with $\gamma = 1778$). At an indentation of $0.13R$ the mechanical response of the pentamers suddenly decreases due to shape inversion, see Fig. 4B. Linear spring constants are determined by fitting the region of small ξ , implying $F = 258\xi$ for pentamers and $F = 139\xi$ for hexamers. The inset displays the same curve as it would be measured in an experiment with an elastic cantilever with spring constant $K_c = 100$.

Eq. (4) for $\gamma > 10$, see Fig. 1 in the supplementary material. For $\gamma < 10$ the scaling picture breaks down since the dominant bending energy is no longer concentrated in a small region around the pole.

At a critical indentation $\xi_c \sim h/R \sim \gamma^{-1/2}$ the shell undergoes a larger shape transformation in which a circular region in the upper part inverts its shape, see Fig. 4B. Here, the deformation energy is concentrated in a ring of radius r and width d . The radius of curvature of the ring is $\sim Rd/r$ and meridians are shortened by a factor $\sim rd/R^2$. By using again d to equilibrate bending and elastic energy (i.e. $d \sim R/\gamma^{1/4}$) one finds $E/\kappa_b \sim \xi^{3/2}\gamma^{1/4}$ leading to a nonlinear force-distance relation $F \sim \xi^{1/2}$.

For sufficiently large γ the inversion transition of pentamers (shown in Fig. 4B) is a first order transition (in ξ) as can be seen from the $F(\xi)$ -curve in Fig. 2C. There, only the green lines correspond to conformations of minimal energy. The blue lines represent intermediate (metastable or unstable) conformations connecting the weakly and strongly deformed capsid shapes. For smaller γ the transition is continuous, see Fig. 2B.

With our numerical simulations it is also possible to extract precise material parameters of experimentally investigated viruses. To do so we have simulated the conditions corresponding to the SFM experiments on $\phi 29$ [9]. By using the FvK number γ as fit parameter for the measured bimodality ratio $K_i^{\text{pent}}/K_i^{\text{hex}} \simeq 1.88$ one finds $\gamma \simeq 1778$, in good agreement with the value estimated above from the geometrical parameters of Ref. [26].

Then, $\kappa_b/R^2 \simeq 1.14\text{mN/m}$ can be extracted directly from the dimensionless spring constant $K_l \equiv k_l R^2/\kappa_b$ shown in Fig. 3 by using, e.g., the softest experimentally measured value of $k_l = 0.16\text{N/m}$ (with corresponding $k_l^{\text{pent}} = 0.296\text{N/m}$) [9]. The force scale is then $\kappa_b/R \simeq 24\text{pN}$. For empty CCMV the bimodality cannot be resolved experimentally ($k_l = 0.15 \pm 0.01\text{N/m}$ [10]), while numerically we find $k_l^{\text{hex}} = 0.17\text{N/m}$ and $k_l^{\text{pent}} = 0.12\text{N/m}$. In this case, we extract $\kappa_b/R^2 \simeq 2.4 \pm 0.2\text{mN/m}$ and $\kappa_b/R \simeq 29 \pm 2\text{pN}$ from the numerical data.

With these material parameters a direct comparison with SFM experiments can be achieved. Fig. 5 shows as an example the force-distance curves for hexamers and pentamers of $\phi 29$. Within our numerical analysis it is even possible to take into account the elastic spring constant of the cantilever K_c (measured in units of κ_b/R^2). Then, a measured force F corresponds to a displacement $X'/R = F/K_c + \xi$ of the shell. Thus, as Fig. 5 shows for sufficiently stiff cantilevers the shape inversion of the viral shell leads to a discontinuous force-displacement curve. The numerical results (shown in the inset) are in excellent agreement with the experimentally measured force-distance curves [9]. In particular, for both numerical and experimental deformations the shape instability occurs at $\xi_c \simeq 0.13$.

Rupture. We have also analyzed the *local* response of elastic shells to loading by investigating the conditions under which rupture occurs. This process takes place in regions of high in-plane stress where bonds break due to over-stretching or compression. Thus, this analysis provides information about the interaction between capsomers.

As experimentally observed, phage $\phi 29$ breaks at a critical indentation $X_r \simeq 7.7\text{nm} \simeq 0.35R$ [9]. To determine the associated change in bond length we have calculated numerically the shape of a shell with $\gamma = 1778$ at this indentation yielding a maximal compression of $\simeq 4.5\%$. The corresponding numerical rupture force is $f_r \simeq 43\kappa_b/R \simeq 1.0\text{nN}$ in agreement with experimental findings [9]. Using this criterion, the numerics for empty CCMV predicts a rupture force $f_r \simeq 22\kappa_b/R \simeq 0.57\text{nN}$ while the experimentally determined value is $f_r \simeq 0.63\text{nN}$ [10].

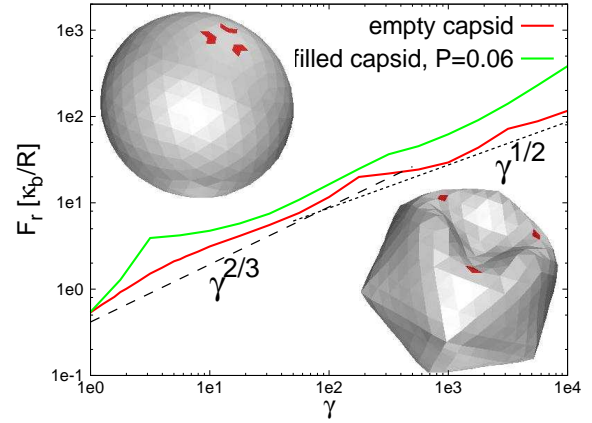


Fig. 6. (Dimensionless) rupture force of an icosahedral capsid with (green curve) and without (red curve) volume constraint. Rupture is assumed to occur at a critical bond length change of 4.5%. The rupture force increases with γ since it becomes harder to stretch/compress the material. The rupture force shows a γ^α dependence. We find $\alpha = 0.65 \pm 0.03 \simeq 2/3$ for low γ and $\alpha = 0.53 \pm 0.04 \simeq 1/2$ for large γ . The crossover takes places at the inversion transition shown in Fig. 4. The insets show ruptured structures for $\gamma = 10$ and $\gamma = 3162$. The bonds where rupture occurs first are shown as red diamonds.

In the following, we analyze rupture of viral shells as a function of γ . Fig. 6 shows the γ -dependence of f_r . For $\gamma < 100$ rupture occurs in the linear regime, see Fig. 4A. Here, rupture is caused by compression of meridians, see left inset in Fig. 6. In the linear regime, we observe that the rupture force scales approximately $\sim \gamma^{2/3}$. However, most viruses have higher FvK numbers and will therefore rupture in the nonlinear regime after shape inversion, see Fig. 4B. Here, rupture is caused by circumferential compression in the highly bent rim. In this regime, the rupture force scales (roughly) $\sim \gamma^{1/2}$.

We have also investigated the influence of the capsid geometry

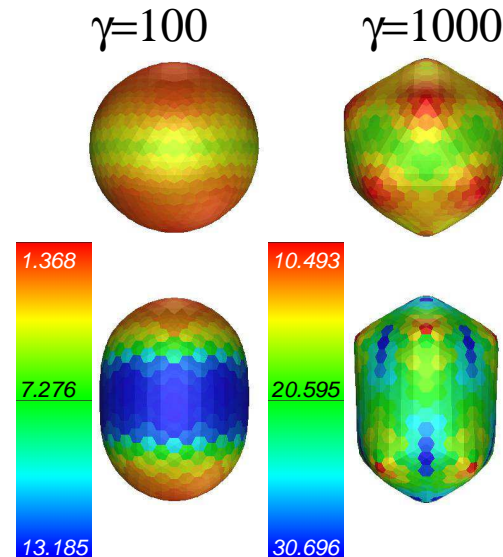


Fig. 7. Rupture force in units of κ_b/R plotted across the surface of spherical and spherocylindrical capsids with $\gamma = 100$ and $\gamma = 1000$. Rupture is assumed to occur at a critical bond length change of 4.5%.

on rupture by comparing an icosahedral and a sphero-cylindrical capsid. This is motivated by the fact that even-numbered T -phages and $\phi 29$ have additional capsomers in the equatorial region elongating the icosahedral shape. For example, the head of $T4$ is an icosahedron with triangulation number 13 and one additional ring of hexamers [31]. The geometry of the sphero-cylinder used in our simulations is that of $\phi 29$, i.e. an icosadeltahedron with triangulation number 3, elongated by two additional equatorial rings of radius R [26]. The force was applied perpendicularly to the axis of symmetry. In order to avoid tilting of the structure, the lowest 10% of vertices of the shell were kept fixed in the simulations.

Fig. 7 shows the rupture force mapped across the surface for $\gamma = 100$ and $\gamma = 1000$. In the corresponding numerical simulations every vertex was indented in steps of $R/250$ followed by the calculation of the new equilibrium conformation. When stretching of some bond exceeded 4.5% the applied force was determined. For $\gamma < \gamma_b$ below the buckling threshold the shells have a uniform elastic behavior across the surface. Since the force exerted on the caps has a tangential component, part of the displacement directly leads to bond stretching. Therefore, the caps are the regions of highest instability. Above the buckling threshold, the pentamers are rigid cones but the space between them becomes more flexible. When pushing a pentameric region the displacement is mainly transformed into compression of the ridges. Pentamers are thus the most unstable region. On average a larger (scale-free) force is required to break the capsid for larger FvK number γ .

The spatial distribution of deformation energy can serve as a measure for the tendency to rupture. To mimic an ensemble of indentation experiments, we carried out simulations in which each vertex of the shell was indented by a constant ξ ($\xi = 0.1$). For all vertices the deformation energy was recorded for all deformations. In order to find the spatial distribution of deformation energy in the ensemble, the elastic energy per vertex was averaged over the ensemble measurement. Fig. 8 shows a map of the average spatial distribution of elastic energy,

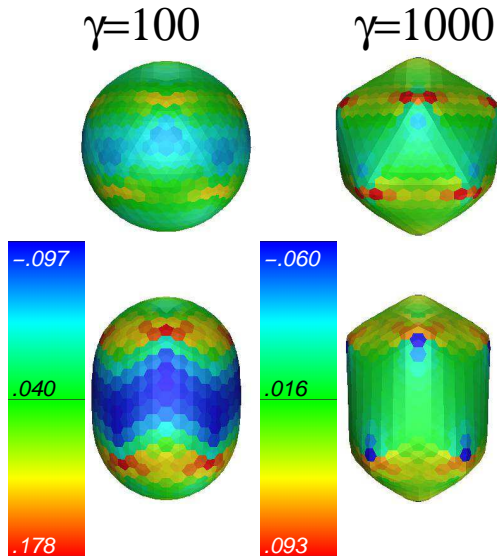


Fig. 8. Averaged distribution of elastic deformation energy for an ensemble measurement where every vertex was indented by an amount $\xi = 0.1$. In the simulations, loading was perpendicular to the axis of symmetry. The ensemble average shows that the elastic energy is concentrated in a small region just below the caps. The capsid will most likely break in this region.

normalized by the total elastic energy put into the system during the measurement on the ensemble.

In our simulations we assume a uniform distribution of binding energies between capsomers. In reality, binding energies will show a spatial variation and an ensemble of indentation experiments on capsids will yield different rupture probabilities than the numerical data presented in Fig. 8. However, with a direct comparison of the two approaches conclusions about the distribution of binding potentials can be drawn.

Filled Capsids. Phages infect their host cells by penetrating the cell membrane and rapidly injecting the DNA into the cell plasma. Therefore, their DNA is stored under high pressure. The pressure p of DNA inside $\phi 29$ is of the order of $p \simeq 6\text{MPa}$ [1, 5] or in units of elastic parameters $p \simeq 0.06\kappa_e/R$.

Other viruses, like CCMV, self-assemble inside the host cell and enclose the DNA. Correspondingly, their internal pressure is much lower than that of phages. Typically, $p = 1\text{atm} = 0.01\kappa_e/R$ is a good estimate for the internal pressure of a filled CCMV capsid.

To investigate the influence of internal pressure on the elastic properties we have numerically simulated filled capsids with the methods described above. However, here the additional constraint has to be taken into account that due to the presence of DNA inside the capsids the enclosed volume is fixed. In order to mimic a packed $\phi 29$ phage, first the equilibrium conformation under pressure was determined by minimizing the total energy with an additional pressure contribution $E_p = pV$ with $p = 0.06\kappa_e/R$.

Experiments on full CCMV were performed in Ref. [10]. A direct comparison of our numerical simulations with these experiments yields (for $p = 0.01\kappa_e/R$ and volume $V = \text{const.}$) the spring constants $k_l^{\text{hex}} \simeq 0.19\text{N/m}$, $k_l^{\text{pent}} \simeq 0.12\text{N/m}$, and a rupture force $f_r^{\text{full}} \simeq 0.83\text{nN}$. These values are again in good agreement with the experimental findings ($k_l = 0.20 \pm 0.02\text{N/m}$ and $f_r^{\text{full}} = 0.81 \pm 0.04\text{nN}$). There are no SFM-experiments on filled $\phi 29$ phages to which we could compare our numerical simulations.

Generally, the volume constraint leads to increased linear spring constants, see Fig. 3. This can be understood in the scaling picture: In order to preserve constant cross-sectional area, the local compression at the point of loading must be compensated by an expansion of the equatorial area. Therefore the influence of the volume constraint becomes more apparent for larger γ , i.e. for shells dominated by elastic energy.

At high pressures the circumferential stress at the fivefold discli-

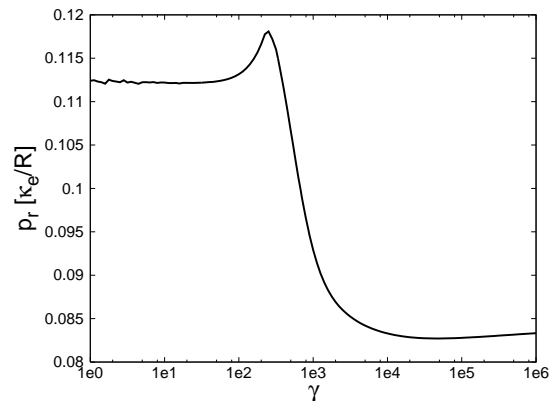


Fig. 9. Rupture pressure (i.e. pressure at which the relative bond stretching reaches 4.5%) for an icosahedral shell as function of γ .

nations is balanced by the volume contribution pV . Thus, pentamers do not form rigid buckles and hexamers remain flat. For example, the DNA pressure of ϕ 29-phages reduces its asphericity a from $a \simeq 1.4 \cdot 10^{-3}$ for an empty capsid to $a \simeq 0.6 \cdot 10^{-3}$. This similarity between hexamers and pentamers is reflected by the fact, that the elastic response of hexamers and pentamers becomes similar for high internal pressure, see Fig. 3.

The rupturing behavior of filled capsids is shown in Fig. 6. The rupture force is larger for filled capsids than for empty ones. Due to the internal pressure the non-indented shell is already stretched. This compensates the force-induced compression in meridional direction at the poles thus reducing their tendency to rupture. Rupture of filled capsids is caused by circumferential expansion at the equator.

Osmotic Shock. One way to extract DNA from viral capsids is to put them under osmotic shock. Under these conditions some viral capsids (e.g. T -even phages) rupture [32] while others (e.g. T -odd phages) stay intact. Thus, these experiments also elucidate details about capsomer-capsomer interactions and we have analyzed whether rupture induced by internal pressure and by external force are related.

To do so we have numerically determined the shape of the capsid under internal pressure p and measured the bond length between neighboring vertices. It was assumed that at rupture pressure the critical bond stretching is 4.5% as for rupturing due to bond compression. Fig. 9 shows the corresponding rupture pressure p_r (in units of κ_e/R) as function of γ for an icosahedral shell.

As can be seen from Fig. 9, capsids with a buckled ground state ($\gamma > \gamma_b$) rupture at lower p_r than unbuckled ones. One should note, that for rupture induced by an external force, rupture forces are generally higher for $\gamma > \gamma_b$ than for $\gamma < \gamma_b$, see Fig. 6. However, as can be seen from the inset in Fig. 6, in the buckled configuration the force-induced deformation propagates over a larger area than in the unbuckled state. Therefore, it is possible that the external rupture pressure for force-induced rupture is also lower for buckled capsids. But this questions needs to be addressed in a more detailed analysis.

For small γ the rupture pressure reaches a constant value, see Fig. 9. In this limit deviations from spherical shape are small and the internal pressure simply leads to a form-invariant up-scaling of the viral shell. Thus, changes in bending energy can be neglected. By equi-

librating the expanding pressure force and the restoring force arising from bond stretching for a triangulated sphere the relative change of bond length is found to be $pR/(3\kappa_e)$. The numerically found value is somewhat lower caused by the small deviations from spherical shape. The same calculation shows that a triangulated sphere with a harmonic stretching energy is only stable for pressures $p < 0.75\kappa_e/R$, independently of γ , see supporting information.

Summary and Conclusions. Recent SFM-measurements have revealed the elastic properties and mechanical limits of viral capsids. In this paper, we have shown that numerical simulations are a powerful tool in complementing these experimental efforts. We have examined the reversible and irreversible mechanical behavior on local and global scales. In particular, we have shown that the elastic parameters characterizing the mechanical properties of phages and viruses can be determined very precisely by a direct comparison of numerical and experimental data. With the numerical methods presented here, one is able to resolve the mechanical response of viral shells in an external force in high detail. In particular, since we are able to distinguish the response of hexamers and pentamers we can identify the origin of the experimentally observed bimodality of the elastic spring constants. We also make predictions for the elastic response and rupturing behavior of both empty and filled capsids as function of the FvK number γ . Furthermore, in our simulations the mechanical limits of viral shells can be probed in an ensemble where every capsomer is indented. The comparison of the corresponding rupture map of the shells with experimental data on SFM-induced rupturing offers new methods in experimentally probing the local protein-protein interactions. We can also use the rupture criterion to predict the maximal sustainable internal pressure of capsids.

So far, we have focused on shells with the shape of an icosahedron. However, many viruses such as phage HK97 [33] or the animal virus polyoma [34] are chiral. The influence of chirality on the elastic properties and mechanical stability will be addressed in a forthcoming publication [30].

Acknowledgment. PL gratefully acknowledges support through the Fonds der Chemischen Industrie and the Center for Theoretical Biological Physics (National Science Foundation Grants Nos. PHY0216576 and PHY0225630).

- Smith, D. E., Tans, S. J., Smith, S. B., Grimes, S., Anderson, D. L., & Bustamante, C. (2001) *Nature* **413**, 748–752.
- Riemer, S. C. & Bloomfield, V. A. (1978) *Biopolymers* **17**, 785–794.
- Kindt, J., Tzili, S., Ben-Shaul, A., & Gelbart, W. M. (2001) *Proc. Natl. Acad. Sci.* **98**, 13671–13674.
- Tzili, S., Kindt, J. T., Gelbart, W. M., & Ben-Shaul, A. (2003) *Biophys. J.* **84**, 1616–1627.
- Purohit, P. K., Kondev, J., & Phillips, R. (2003) *Proc. Natl. Acad. Sci.* **100**, 3173–3178.
- Purohit, P. K., Inamdar, M. M., Grayson, P. D., Squires, T. M., Kondev, J., & Phillips, R. (2005) *Biophys. J.* **88**, 851–866.
- Atlas, R. M. (1998) *Principles of Microbiology*. (Wm.C. Brown Publishers).
- Evilevitch, A., Lavelle, L., Knobler, C. M., Raspaud, E., & Gelbart, W. M. (2003) *Proc. Natl. Acad. Sci.* **100**, 9292–9295.
- Ivanovska, I., de Pablo, P., Ibarra, B., Sgalari, G., MacKintosh, F., Carrascosa, J., Schmidt, C., & Wuite, G. L. (2004) *Proc. Natl. Acad. Sci.* **101**, 7600–7605.
- Michel, J., Ivanovska, I., Gibbons, M., Klug, W., Knobler, C., Wuite, G. L., & Schmidt, C. (2006) *Proc. Natl. Acad. Sci.* **103**, 6184–6189.
- Caspar, D. & Klug, A. (1962) *Cold Spring Harb. Symp. Quant. Biol.* **27**.
- Lidmar, J., Mirny, L., & Nelson, D. R. (2003) *Phys. Rev. E* **68**, 051910.
- Kumar, A., Reddy, V. S., Yusibov, V., Chipman, P. R., Hata, Y., Fita, I., Fukuyama, K., Rossmann, M. G., Loesch-Fries, L. S., Baker, T. S., & Johnson, J. E. (1997) *J. Virol.* **71**, 7911–7916.
- Olson, N. H., Gingery, M., Eiserling, F. A., & Bakera, T. S. (2001) *Virology* **279**, 385–391.
- Xiao, C., Chipman, P. R., Battisti, A. J., Bowman, V. D., Renesto, P., Raoult, D., & Rossmann, M. G. (2005) *J. Mol. Biol.* **353**, 493–496.
- Dubois, M., Deme, B., Gulik-Krzywicki, T., Dedieu, J.-C., Vautrin, C., Desert, S., Perez, E., & Zemb, T. (2001) *Nature* **411**, 672–675.
- Elsner, N., Dubreuil, F., Weinkamer, R., Wasicek, M., Fischer, F., & Fery, A. (2006) *Prog. Colloid Polym. Sci.* **132**, 117–123.
- Vliegthart, G. A. & Gompper, G. (2006) *Biophys. J.* **91**, 834–841.
- Seung, H. & Nelson, D. R. (1988) *Phys. Rev. A* **38**, 1005–1018.
- Reddy, V., Giesing, H., Morton, R., Kumar, A., Post, C., Brooks III, C., & Johnson, J. (1998) *Biophys. J.* **74**, 546–558.
- Zandi, R., Reguera, D., Bruinsma, R. F., Gelbart, W. M., & Rudnick, J. (2004) *Proc. Natl. Acad. Sci.* **101**, 15556–15560.
- Zandi, R. & Reguera, D. (2005) *Phys. Rev. E* **72**, 021917.
- Wintz, W. (1997) Ph.D. thesis (Universität Potsdam).
- Press, W., Teukolsky, S. A., Vetterling, W. T., & Flannery, B. P. (1992) *Numerical Recipes in C*. (Cambridge University Press).
- Speir, J. A., Munshi, S., Wang, G., Baker, T. S., & Johnson, J. E. (1995) *Structure* **3**, 63–78.
- Tao, Y., Olson, N. H., Xu, W., Anderson, D. L., Rossmann, M. G., & Baker, T. S. (1998) *Cell* **95**, 431–437.
- Lobkovsky, A. E. & Witten, T. (1997) *Phys. Rev. E* **55**, 1577–1589.
- DiDonna, B. & Witten, T. (2001) *Phys. Rev. Lett.* **87**, 206105.
- Landau, L. & Lifshitz, E. (1975) *Theory of Elasticity*. (Pergamon, New York).
- Bünemann, M. & Lenz, P. (2006) to be published.
- Fokine, A., Chipman, P. R., Leiman, P. G., Mesyanzhinov, V. V., Rao, V. B., & Rossmann, M. G. (2004) *Proc. Natl. Acad. Sci.* **101**, 6003–6008.
- Anderson, T. F. (1950) *J. Appl. Phys.* **21**, 70.
- Helgstrand, C., Wikoff, W., Duda, R., Hendrix, R., Johnson, J., & Liljas, L. (2003) *J. Mol. Biol.* **334**, 885–899.
- Stehle, T. & Harrison, S. (1996) *Structure* **4**, 183–194.